Special Double Issue Article

Christian Dreßler, Arne Bochmann, Thomas Schulz, Timmy Reimann, Jörg Töpfer and Steffen Teichert*

Transversal Oxide-Metal Thermoelectric Device for Low-Power Energy Harvesting

Abstract: The concepts of dual leg, unileg and transversal oxide thermoelectric harvesting devices were compared with regard to the dimensionless figure of merit calculated from published data on common dual leg oxide thermoelectric generators. The analysis shows that the application of the transversal thermoelectric effect does not significantly reduce the expected electrical output power density of thermoelectric devices utilizing thermoelectric oxides. At the same time, the transversal device layout is simple in comparison to the common dual leg device. A transversal thermoelectric harvester consisting of a tilted multilayer stack $La_{1.97}Sr_{0.03}CuO_4$/Ag was prepared and analyzed in detail. Simulations using the finite elements method were performed to verify the results. Based on this data, the electrical power density of the transversal oxide-metal device is estimated to be in the range of currently published data on oxide dual leg devices, thus allowing energy harvesting for low power applications.

Keywords: thermoelectric oxide, transversal thermoelectric effect, anisotropic thermoelectric, electrical and thermal transport properties, multilayer technology

DOI 10.1515/ehs-2014-0056

Introduction

Ceramic materials have been in the focus of thermoelectric application for almost 20 years (Ohtaki et al. 1995; Terasaki, Sasago, and Uchinokura 1997). Although the thermoelectric performance data of thermoelectric oxides are inferior to classic thermoelectric materials based on BiTe/PbTe semimetallic alloys, some aspects related to potential application conditions, particularly the stability at high temperatures of a number of ceramic thermoelectric materials, still induce a large number of studies that aim of improving the material properties. This is accompanied by research efforts to implement oxide materials in thermoelectric devices (Shin et al. 2000; Matsubara et al. 2001; Funahashi et al. 2004; Noudem et al. 2008; Tomeš et al. 2010; Feldhoff and Geppert 2014). The integration of oxide materials for thermoelectric harvesting devices typically includes monolithic blocks of n- and p-type ceramics. Alternatively, large-scale ceramic multilayer technology represents an attractive option to manufacture oxides thermoelectric generators (TEG). Ceramic multilayer technologies, including low-temperature co-firing, are well established for the industrial production of electronic components, e.g. resistors, capacitors, inductors and microsystems (Imanaka 2005). Recently, Hayashi et al. (2010) and Funahashi et al. (2011) demonstrated the preparation of monolithic TEG based on a multilayer co-fired ceramic technology. To build up a multilayer-type TEG it is necessary to combine and co-fire p-type and n-type thermoelectric oxides, an insulating material as well as a suitable metal to connect the thermoelectric layers accordingly. Alternatively, the internal contacts between the p- and n-layers can be realized without using an additional metal component (Hayashi et al. 2010, Funahashi et al. 2011). However, in this case it has to be ensured that the direct contacts between the p- and n-materials exhibit a low-contact resistance. Critical material and process parameters for the application of ceramic multilayer technologies are the shrinkage and sintering behaviors of the different ceramic green tapes. In addition, thermal expansion mismatch must be avoided. Implementation of these constraint conditions may reduce the performance reached for individually optimized thermoelectric materials. The reduction of the number of components used for co-firing a ceramic multilayer TEG and, hence, reducing the complexity of the device fabrication, may therefore be beneficial for the performance of the TEG.

In this paper, we discuss various TEG device concepts assuming the application of ceramic multilayer technologies

***Corresponding author: Steffen Teichert,** University of Applied Sciences Jena, Carl Zeiss Promenade 2, 07745 Jena, Germany, E-mail: steffen.teichert@fh-jena.de
Christian Dreßler: E-mail: christian.dressler@fh-jena.de,
Arne Bochmann, Thomas Schulz, Timmy Reimann, Jörg Töpfer, University of Applied Sciences Jena, Carl Zeiss Promenade 2, 07745 Jena, Germany

for the fabrication of low-power energy harvesting generator systems. The assessment of TEG concepts is conducted with special emphasis on possible simplifications of the device layout and not exclusively driven by the premise of a maximum thermodynamic efficiency. Simple thermoelectric devices may show enhanced long-term reliability and low production costs, while at the same time generating sufficient output power to drive sensor or radio applications. A simple theoretical description is used to compare different device concepts, i.e. dual-leg, unileg and transversal multilayer TEGs. A simple transversal thermoelectric energy harvester was prepared. Its thermoelectric performance was evaluated and compared with simulations.

Theoretical Background and Device Concepts

In this section, the theoretical background of three different device concepts feasible within the multilayer technology is evaluated: (i) dual leg thermocouple; (ii) unileg thermocouple; and (iii) transversal thermocouple (Figure 1). The dual leg thermocouple corresponds to the usual setup of thermoelectric devices consisting of p- and n-type conducting thermoelectric materials. The unileg thermocouple follows the same setup. However, in this case a metal is used in combination with a thermoelectric oxide (Lemonnier et al. 2008). The dual leg as well as the unileg device can be addressed using the same theoretical framework. The transversal TEG contains two different materials in an alternating layer stack. The layer stack is tilted at a certain angle with respect to the applied temperature gradient. The transversal device will be discussed assuming a material combination of a thermoelectric oxide and a metal for the alternating layers.

In the case of dual leg as well as unileg devices the electrical and the thermal current flows are aligned in parallel (longitudinal thermoelectric effect), whereas in a transversal thermocouple the electrical current is oriented perpendicularly to the external temperature gradient.

In order to compare these three device concepts the dimensionless figure of merit $Z\bar{T}$ is used (Ioffe 1957). It is worthwhile to mention that $Z\bar{T}$ is derived from thermodynamic considerations, thus defining an upper limit of the expected thermoelectric performance data. For the thermocouple combining n- and p-type conducting thermoelectric materials having Seebeck coefficients S_p, S_n, thermal conductivity λ_p, λ_n and electrical resistivity ρ_p, ρ_n, the maximum figure of merit $Z^{\max}_{\text{long}}\bar{T}$ of the common longitudinal thermoelectric effect can be written as follows:

$$Z^{\max}_{\text{long}}\bar{T} = \frac{(S_p - S_n)^2}{\left(\sqrt{L_p} + \sqrt{L_n}\right)^2} \quad [1]$$

with $L_p = \rho_p\lambda_p/\bar{T}$ and $L_n = \rho_n\lambda_n/\bar{T}$ as Lorenz numbers of the n- and p-type material respectively. Equation [1] is valid only if the following condition is fulfilled:

$$\frac{h_n A_p}{h_p A_n} = \sqrt{\frac{\rho_p \lambda_n}{\rho_n \lambda_p}} \quad [2]$$

using h_n, h_p and A_n, A_p for the height and the cross section of the individual thermocouples (Goldsmid 1995). A further performance parameter is the maximum electrical output power per unit area $w^{\max}_{\text{long}}$. If the internal resistance of the thermoelectric device R_i matches the external load R_{load}, the maximum electrical power per unit area $w^{\max}_{\text{long}}$ is calculated by (Cobble 1995):

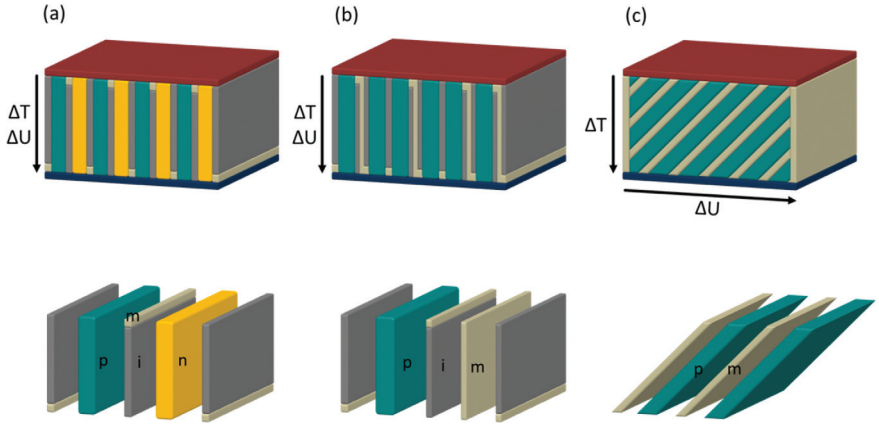

Figure 1: Scheme of the layer stack for (a) dual leg, (b) unileg and (c) transversal thermoelectric device; ΔT – temperature gradient; ΔU – voltage drop; p – p-type thermoelectric oxide; n – n-type thermoelectric oxide; i – isolator; m – metal.

$$w_{\text{long}}^{\max} = \frac{(S_p - S_n)^2 \Delta T^2}{4h\left(\sqrt{\rho_p} + \sqrt{\rho_n}\right)^2} \quad [3]$$

containing only h as geometrical parameter for the height of the device parallel to the temperature gradient. Equation [3] presumes the fulfillment of the condition:

$$\frac{h_n A_p}{h_p A_n} = \sqrt{\frac{\rho_p}{\rho_n}} \quad [4]$$

Equations [1]–[4] describe the longitudinal thermoelectric effect, thus the dual leg as well as unileg devices, respectively. In the latter case one set of transport parameters has to be replaced by the metal parameters S_{met}, λ_{met} and ρ_{met}.

Apart from common longitudinal thermoelectric effect described, the existence of a transversal thermoelectric effect was shown theoretically (Voigt 1910) and experimentally (Reddemann 1937) a long time ago. In this case, the temperature gradient is aligned perpendicularly to the resulting electrical potential (Figure 1(c)). The prerequisite of the occurrence of this effect is anisotropy of the electrical transport in the thermoelectric material. Particularly single crystals (Gallo, Chandrasekhar, and Sutter 1963) or epitaxially grown layers (Schnellbögl et al. 1992; Kanno et al. 2014) with native anisotropic electrical properties are suitable to generate a transversal thermoelectric potential. The possibility to use artificially created anisotropic materials for thermoelectric power generators based on the transverse thermoelectric effect was elaborated theoretically in detail by Babin et al. in 1974 (Babin et al. 1974). Initial experimental data on tilted layer stacks of $Bi/Bi_{0.5}Sb_{1.5}Te_3$ were published by Gudkin et al. in 1978 (Gudkin, Iordanishvili, and Fiskind 1978). It also has to be mentioned that the application of anisotropic thermoelectric materials has been discussed recently (Snarskii and Bulat 2006; Reitmaier, Walther, and Lengfellner 2010; Goldsmid 2012; Takahashi et al. 2013, Zhou et al. 2013).

For the further discussion, the combination of a thermoelectric oxide and a metal will be supposed. The oxide-metal layer stack is tilted at the angle φ with respect to the applied temperature gradient. Starting with a set of material transport coefficients $S_{ox}, \lambda_{ox}, \rho_{ox}$ and $S_{met}, \lambda_{met}, \rho_{met}$ for the individual oxide and metal layers at a thickness ratio of $r_t = t_{met}/t_{ox}$ the calculation of two sets of transport properties parallel and perpendicular to the layer stack results in (Babin et al. 1974):

$$S_\perp = \frac{\lambda_{met} S_{ox} + r_t \lambda_{ox} S_{met}}{r_t \lambda_{ox} + \lambda_{met}} \quad S_\parallel = \frac{\rho_{met} S_{ox} + r_t \rho_{ox} S_{met}}{r_t \rho_{ox} + \rho_{met}} \quad [5a, b]$$

$$\lambda_\perp = \frac{\lambda_{ox}\lambda_{met}(1 + r_t)}{r_t \lambda_{ox} + \lambda_{met}} \quad \lambda_\parallel = \frac{\lambda_{ox} + r_t \lambda_{met}}{1 + r_t}\left(1 + Z_{\text{long}}\bar{T}\right) \quad [6a, b]$$

$$\rho_\perp = \frac{\rho_{ox} + r_t \rho_{met}}{1 + r_t} \quad \rho_\parallel = \frac{\rho_{ox}\rho_{met}(1 + r_t)}{r_t \rho_{ox} + \rho_{met}} \quad [7a, b]$$

with the not maximized figure of merit $Z_{\text{long}}\bar{T}$ of the longitudinal thermocouple consisting of the same materials:

$$Z_{\text{long}}\bar{T} = \frac{r_t (S_{ox} - S_{met})^2 \bar{T}}{(\lambda_{ox} + r_t \lambda_{met})(r_t \rho_{ox} + \rho_{met})} \quad [8]$$

The parameters of interest are the Seebeck coefficient S_{xy} with the temperature gradient applied parallel to the y-axis and a potential drop parallel to the x-axis (Figure 2), the thermal conductivity parallel to the y-axis λ_{yy} and the electrical resistivity parallel to the x-axis ρ_{xx}:

$$S_{xy} = \left(S_\perp - S_\parallel\right) \cos\varphi \sin\varphi \quad [9]$$

$$\lambda_{yy} = \lambda_\perp \sin^2\varphi + \lambda_\parallel \cos^2\varphi \quad [10]$$

$$\rho_{xx} = \rho_\perp \cos^2\varphi + \rho_\parallel \sin^2\varphi \quad [11]$$

The resulting figure of merit of the transversal thermoelectric effect $Z_{tr}\bar{T}$ can be written as

$$Z_{tr}\bar{T} = \frac{S_{xy}^2}{\lambda_{yy}\rho_{xx}}\bar{T} \quad [12]$$

Using the conditions

$$\lambda_{ox} \ll \lambda_{met} \text{ and } \rho_{ox} \gg \rho_{met} \quad [13]$$

Babin et al. (1974) derived a simplified expression for the maximum figure of merit $Z_{tr}^{\max}$ obtained for the tilt angle

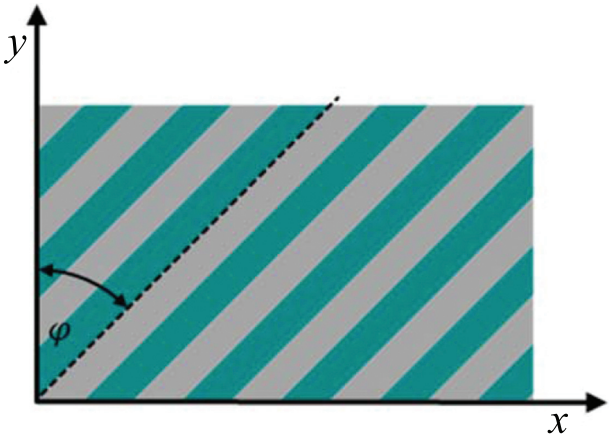

Figure 2: Illustration for the definition of the coordinate system for the theoretical description of the transversal thermocouple consisting of alternating stacked materials.

$\varphi_{\max}$. Condition [13] is easily satisfied for the considered material combination of thermoelectric oxide and metal. For this material combination $Z_{tr}^{\max}$ and $\varphi^{\max}$ can be expressed as follows:

$$Z_{tr}^{\max}\bar{T} = \frac{(S_{ox} - S_{met})^2}{\left(\sqrt{L_{ox}} + \sqrt{L_{met}\left(1 + Z_{\log}\bar{T}\right)}\right)^2} \quad [14]$$

$$tan\varphi^{\max} = \frac{\sqrt{r_t}}{r_t + 1}\sqrt[4]{\frac{\lambda_{met}\rho_{ox}}{\rho_{met}\lambda_{ox}}\left(1 + Z_{\log}\bar{T}\right)} \quad [15]$$

Equation [14] reveals that the figure of merit $Z_{tr}^{\max}$ of the transversal thermocouple is always smaller than the figure of merit $Z_{\log}^{\max}$ (eq. [1]) of a longitudinal thermocouple consisting of the same material pair. However, as already discussed by Goldsmid (2012), in the case of a small figure of merit this reduction is not significant. Furthermore, the Lorenz number of the metal L_{met} for the unileg device is typically one order of magnitude smaller compared to L_{ox} of thermoelectric oxides, thus additionally reducing the influence of the denominator of eq. [14] on $Z_{tr}^{\max}$.

The estimated thickness ratio $r_t^{\max}$ for the maximum figure of merit is (Babin et al. 1974):

$$r_t^{\max} = \sqrt{\frac{2L_{met}/L_{ox}}{1 + L_{met}/L_{ox}}} \quad [17]$$

If the internal resistance of the transversal thermocouple is equal to the external load then the electrical power per unit area can be expressed as

$$w_{tr} = \frac{S_{xy}^2\Delta T^2}{4h\rho_{xx}} \quad [18]$$

with h for the height of the thermocouple parallel to the temperature gradient.

In order to discuss the performance potential of the different device types, previously published data on full oxide dual leg devices are used. The transport properties of the corresponding thermoelectric oxides were estimated in the low (300–400 K) and medium temperature (800 K) range. For some devices no thermal conductivity data of the materials used was given in the original reports of the devices. In these cases the thermal conductivity was estimated based on additional literature describing similar materials. The metal transport properties were estimated assuming the application of a commercial Ag paste typically used in ceramic multilayer technology (Heraeus 2014). The room temperature resistivity ρ_{met} is $4.2 \cdot 10^{-8}$ Ωm. The Lorenz number was estimated based on resistivity (Matula 1979) and thermal conductivity (Ho, Powell, and Liley 1972) data of pure Ag as L_{met} 2.4 10^{-8} V^2K^{-2}. The calculation of the temperature dependence of ρ_{met} and λ_{met} was made applying the Wiedemann–Franz law. The Seebeck coefficient vs temperature of Ag was taken from Cusack and Kendall (1958).

Combining all transport data it is possible to calculate the figures of merit of the individual materials (Z_p, Z_n), of the dual leg device $(Z_{\text{dual}}^{\max})$ as well as of the corresponding unileg $(Z_{\text{uni}}^{\max})$ according to eq. [1] for the longitudinal thermoelectric effect. The figure of merit $Z_{tr}^{\max}$ of a transversal device is calculated from the combination of a metal and an oxide. Table 1 summarizes published experimental data of dual leg thermocouples at different temperatures and calculated Z_p and Z_n as well as the ratio $Z_{\text{dual}}^{\max}/Z_{\text{uni}}^{\max}$. The calculation of $Z_{\text{uni}}^{\max}$ was made for the combination of the metal with the oxide exhibiting the higher figure of merit of the p/n material pair. The overview of the data shows that for a number of oxide dual leg devices published so far the corresponding unileg device using only the better performing oxide together with a metal would result in a higher figure of merit than the oxide-oxide couple. Only a small number of dual leg devices exhibit a remarkable advantage over the unileg device showing $Z_{\text{dual}}^{\max}/Z_{\text{uni}}^{\max} > 1.5$. The ratio of the maximized electrical power $w_{\text{dual}}^{\max}/w_{\text{uni}}^{\max}$ behaves in a similar way. This result is a consequence of the typically rather weak coincidence of the transport properties of the oxide pairs used together. Therefore the key parameter for the result of the ratio $Z_{\text{dual}}^{\max}/Z_{\text{uni}}^{\max}$ is not the figure of merit of a single material but only the coincidence of the individual transport properties of the two materials. It also might be difficult in future to improve the match of the thermoelectric properties considering technological requirements at the same time. In such a situation the unileg design using the better performing oxide together with a metal might be the better technological choice.

In a next step the ratio $Z_{\text{dual}}^{\max}/Z_{tr}^{\max}$ is calculated from the data available. This ratio is not separately listed in Table 1 because the result is practically the same as in case of $Z_{\text{dual}}^{\max}/Z_{\text{uni}}^{\max}$, the difference found between these ratios being negligibly small. Hence, the expected figure of merit of unileg and a corresponding transversal thermoelectric device prepared from a thermoelectric oxide and Ag is almost the same. This follows from the large difference of the Lorenz number of Ag in comparison to the oxides and the small value $Z_{\log} \leq Z_{\log}^{\max}$ at a layer thickness ratio r_t optimized for the transversal device according to eq. [17]. The conclusion of the discussion should be summarized as follows: If a typical thermoelectric oxide with a high figure of merit is available and the given partner material does not show matching

Table 1: Summary of published and calculated data for different device structures.

T	p-material	ρ_p	S_p	λ_p	$Z_p\bar{T}$	n-material	ρ_n	$-S_n$	λ_n	$Z_n\bar{T}$	$\frac{Z^{max}_{dual}}{Z^{max}_{uni}}$	$\frac{w^{max}_{dual}}{w^{max}_{uni}}$	Source
K		Ωm	μV/K	W/mK			Ωm	μV/K	W/mK				
400	$Li_{0.025}Ni_{0.975}O$	6.7E-5	80	12.0	3.2E-03	$Ba_{0.4}Sr_{0.6}PbO_3$	1.3E-4	90	2.0	3.2E-5	0.7	1.3	Shin et al. (2000); Shin and Murayama
800	$Li_{0.025}Ni_{0.975}O$	5.0E-5	50	10.0	4.0E-03	$Ba_{0.4}Sr_{0.6}PbO_3$	5.0E-5	100	2.0	1.0E-4	0.5	0.7	(1999); Yasukawa and Murayama (1998)
800	$Ca_{2.75}Gd_{0.25}Co_4O_9$	7.8E-3	185	1.6	2.2E-03	$Ca_{0.92}La_{0.08}MnO_3$	6.6E-3	120	2.0	1.1E-6	0.8	0.8	Matsubara et al. (2001); Liu et al. (2009); Funahashi et al. (2007)
800	$Ca_{2.8}Bi_{0.2}Co_4O_9$	2.0E-4	150	0.6	1.4E-01	$Ca_{0.98}Sm_{0.02}MnO_3$	1.4E-4	180	1.6	1.5E-4	1.9	1.6	Su et al. (2011)
800	$Na(Co_{0.95}Ni_{0.05})_2O_4$	1.3E-4	350	2.0	3.9E-01	$Zn_{0.99}Sn_{0.01}O$	4.7E-5	175	3.0	2.2E-4	1.2	1.0	Park, Choi, and Lee (2009); Wang, Wang, and Zhao (2009); Ohtaki, Araki, and Yamamoto (2009)
400	$La_{1.98}Sr_{0.02}CuO_4$	3.0E-4	270	2.5	3.9E-02	$CaMn_{0.98}Nb_{0.02}O_3$	2.2E-4	200	2.5	7.3E-5	1.1	0.9	Tomeš et al. (2010)
800	$La_{1.98}Sr_{0.02}CuO_4$	4.0E-4	130	1.8	1.9E-02	$CaMn_{0.98}Nb_{0.02}O_3$	3.2E-4	250	1.8	1.1E-4	0.8	0.6	
400	$La_{1.97}Sr_{0.03}CuO_4$	1.5E-4	214	6.0	2.0E-02	$Nd_{1.97}Ce_{0.03}CuO_4$	4.8E-4	158	3.5	1.5E-5	0.7	0.4	Hayashi et al. (2010)
400	$Ca_3Co_4O_9$	3.3E-5	82	1.6	5.0E-02	$Ca_{0.9}Nd_{0.1}MnO_3$	9.1E-5	141	3.5	6.3E-5	1.7	1.2	Lim et al. (2012); Zhang and Zhang (2008); Funahashi et al. (2007)
800	$Ca_3Co_4O_9$	4.5E-5	121	1.6	1.6E-01	$Ca_{0.9}Nd_{0.1}MnO_3$	8.0E-5	167	3.5	1.0E-4	2.1	1.3	
300	$Ni_{0.9}Mo_{0.1}$	1.3E-6	20	6.6	1.4E-02	$La_{0.035}Sr_{0.965}TiO_3$	1.8E-5	153	5.2	2.5E-4	1.3	0.9	Funahashi et al. (2011)
800	$Ca_3Co_{3.8}Ag_{0.2}O_9$	1.1E-4	120	1.0	1.1E-01	$Ca_{0.98}Sm_{0.02}MnO_3$	1.4E-4	180	1.6	1.5E-4	1.7	0.9	Han et al. (2011)
400	$Nd_{0.995}Ca_{0.005}CoO_3$	4.5E-3	450	1.3	1.4E-02	$LaCo_{0.99}Mn_{0.01}O_3$	2.0E-3	100	1.5	3.3E-6	0.6	0.6	Inagoya et al. (2011); Hashimoto, Kusunose, and Sekino (2009); Li and Li (2011)
800	$Ca_{2.76}Cu_{0.24}Co_4O_9$	3.3E-4	220	1.8	6.5E-02	$Ca_{0.8}Dy_{0.2}MnO_3$	9.5E-5	50	1.5	1.8E-5	1.0	0.7	Park and Lee (2013); Wang et al. (2010); Nakamura and Uchida (1993)

transport properties then the corresponding unileg device will give the higher figure of merit. Furthermore, if the unileg is the better choice, then the corresponding transversal device will have almost the same figure of merit and could be chosen as well.

With special emphasis on multilayer technologies the transversal device has the advantage of the application of metal and thermoelectric oxide layers only. No additional oxide layers are required in this case. Only two materials need to be implemented and the electrical contact behavior can be optimized for one oxide metal combination. Furthermore, the complete device volume can be used for the active material. No additional space is needed for insulators or air gaps which may increase the electrical power per unit area. The decoupling of thermal and electrical current flows gives additional degrees of freedom for the extraction of the electrical energy keeping a maximum temperature difference.

Experimental Analysis

In order to evaluate the concept of a thermoelectric transversal generator based on the oxide – metal combination a test vehicle was prepared with usual laboratory equipment. $La_{1.97}Sr_{0.03}CuO_4$ (LSCO) was chosen as thermoelectric oxide because of good thermoelectric properties in the low temperature range (P. Tomeš et al. 2010; Nakamura and Uchida 1993). In addition, the usability in a ceramic multilayer process has already been demonstrated (Hayashi et al. 2010). LSCO polycrystalline samples were prepared using a common solid-state reaction method. The reactants La_2O_3, CuO and $SrCO_3$ were mixed in the stoichiometric ratio and calcinated in air at 1073 K for 6 h. Then the powder was milled, pressed into disc-shape samples applying a pressure of 3 MPa followed by a sintering process at 1273 K for 2 h under air. The Seebeck-coefficient S and electrical resistivity ρ were measured in a LSR-3 Seebeck system (Linseis, Germany). The thermal conductivity λ was calculated from the measured thermal diffusivity α (LFA-1000, Linseis, Germany), the heat capacity c_p (DSC PT1600, Linseis, Germany) and the material density.

A transverse thermoelectric device (TTD) was assembled simply by stacking 19 calcinated discs of LSCO with a thickness of 1.5 mm each using an intermediate commercial silver paste (Heraeus 2014). The layer stack tilt angle was $\varphi = 45°$. Afterwards the layer stack was dried for 24 h at room temperature and annealed at 850°C for 15 min. Finally, the stack was ground and polished to obtain a rectangular shaped

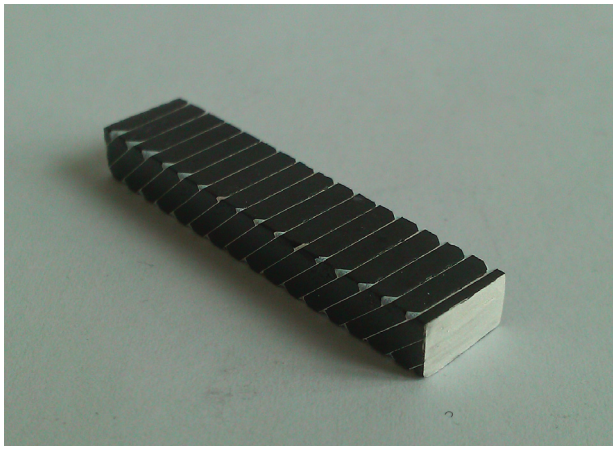

Figure 3: Transversal thermoelectric device prepared with $La_{1.97}Sr_{0.03}CuO_4$ and silver.

TTD with the dimension length × width × height of 36.5 × 8.2 × 4.8 mm^3 (Figure 3). The silver paste was applied manually leading to a certain scattering of the Ag thickness. An average final thickness of the Ag layer of 45 µm was estimated based on the SEM analysis in different positions.

The TTD characterization was carried out in a self-made measurement setup. The TTD was placed between two ceramic blocks with thermal grease. The upper block was heated and the lower ceramic block was only passively cooled by air. This setup does not allow the separate control of the average temperature and the temperature difference. The temperature gradient was directly measured on the upper and lower surface of the sample with two NiCr-Ni-thermocouples (Type-K). Electrical contacting was carried out by a usual four-point probe arrangement with two contacts on each side of the TTD. A four quadrant source-measure unit (Keithley 2400) was used to simulate a tunable load resistance for the TTD. Linear current–voltage (I–V) curves could be obtained indicating ohmic contact behavior of the device. Each I-V curve gives open source voltage V_{oc} and short circuit current I_{sc} for the actual average temperature $\bar{T}$ and the temperature difference ΔT. Using the measured data together with the device dimensions it is possible to derive further parameters such as the resistance of the TTD R_{TTD}, the Seebeck coefficient S_{xy} or the transversal resistivity ρ_{xx}.

For comparison, stationary 2-dim FEM simulations of the TTD were performed with the software COMSOL Multiphysics 4.4 including the thermoelectric node. Mesh-dependent solution convergence was tested giving good results even for coarse meshes. Materials data measured versus temperature were used to derive analytical functions

by regression analysis for LSCO parameters $S_{LSCO}(T)$, $\rho_{LSCO}(T)$ and $\lambda_{LSCO}(T)$. These functions are used for the simulation shown in Figure 4. The corresponding data of Ag were determined as described in chapter 2. Furthermore, measured temperatures as well as geometrical parameters of the prepared TTD were used as further input parameters for the simulation. An exemplary simulation outcome for a measured $\Delta T = 37.4$ K and matched load condition ($R_{TTD} = R_{Load}$, maximum power) is given in Figure 4. The temperature distribution is displayed as color map in Figure 4(a). The electrical potential as well as the electrical current density is shown in (4b) and (4c). Here, the left side of the TTD is set to zero potential. The electrical circuit is closed on the right side of the TTD via the resistance R_{Load}. The contacts are set to equipotential lines accordingly. The electrical potential maps are overlaid by current streamlines Figure 4(b) includes the complete electrical current. In Figure 4(c) the parasitic Eddy currents inside of the device are excluded, thus showing only the fraction of useful electrical current.

Results and Discussion

Transport properties of the LSCO obtained in the temperature range between 300 K and 980 K are shown in Figure 5. The electrical resistivity of LSCO increases with increasing temperature reaching 0.2 mΩm at 980 K indicating a metal-like behavior. The Seebeck coefficient decreases from 230 μV/K to 105 μV/K in the corresponding temperature range. Furthermore, the thermal conductivity slowly decreases with temperatures from 3.0 $Wm^{-1}K^{-1}$ at 300 K to 2.1 $Wm^{-1}K^{-1}$ at 980 K. These results are within expectations considering data published on a

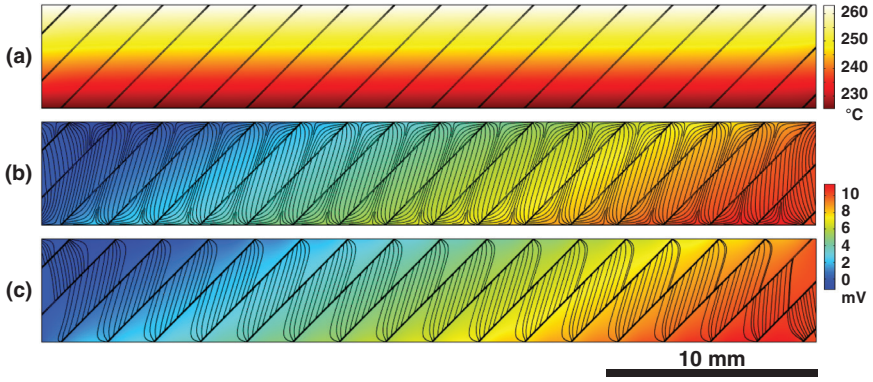

Figure 4: 2D simulation results for matched load ($R_{TTD} = R_{Load}$) and $\Delta T = 37.4$ K. (a) temperature distribution, (b) voltage distribution (color map) and current streamlines, (c) like (b) but with streamlines of useful current only.

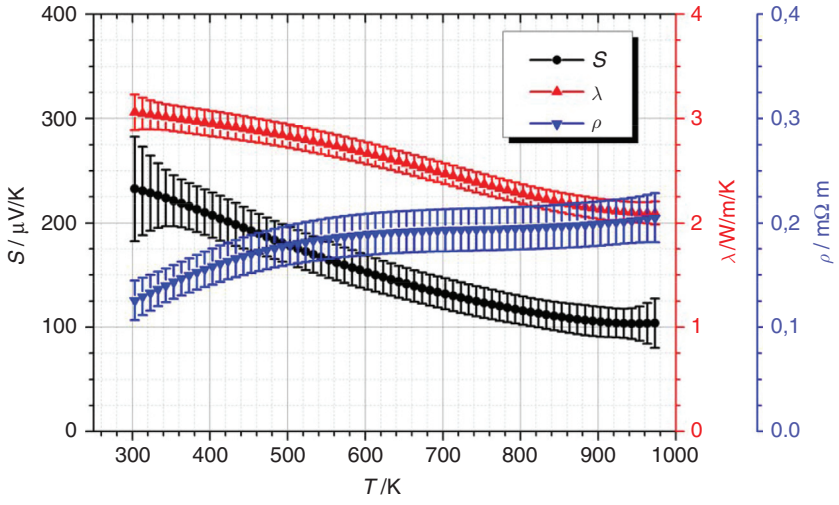

Figure 5: The transport properties Seebeck coefficient S (black), thermal conductivity λ (red) and resistivity ρ (blue) vs temperature of $La_{1.97}Sr_{0.03}CuO_4$ are shown.

thermoelectric oxide of similar composition $La_{1.97}Sr_{0.03}CuO_4$ (Tomeš et al. 2010).

The measurements of the TTD were made in the temperature range from 300 K up to 550 K. The temperature difference ΔT obtained without special measures for cooling of the low temperature side of the TTD rose from 0 K to 37.4 K in this temperature interval. It is clearly evident that measurement conditions with an active cooling of the cold side would lead to larger temperature gradients. However, for this discussion, the characterization conditions used allow the evaluation of the measured and calculated device properties in a sufficient way.

A comprehensive overview of the measured and simulated data of the fabricated TTD is given in Figure 6. In all graphs three data sets are plotted: "theory" indicates the analytically calculated results based on equations from chapter (2) and the raw material data; "simulation" provides results of the FEM calculation, thus representing also calculated data. The measured device data are indicated by "experimental". The measured open circuit voltage U_{oc} does not show the typical linear scaling with increasing temperature due to the change of the average temperature of the TTD and the reduction of the Seebeck coefficient of LSCO at higher temperatures. For the open circuit voltage U_{oc} as well as the short circuit current I_{sc} the simulated data match the experimental data fairly well. The analytically calculated values show a larger deviation compared to the measured data. The reason is related to the limited size of the TTD. The theoretical description by Babin et al. (1974) is an effective medium calculation neglecting border effects which are potentially essential for devices of limited size. The simulation on the other hand includes two crucial size effects: (i) electrical equipotential sides of the TTD (Snarskii, Pal'ti, and Ascheulov 1997) and (ii) a coarsening effect due to the individual layer thicknesses that are not negligible in comparison to the device dimensions (Gudkin and Fiskind 1978). The second effect had also been previously evaluated numerically by Kanno et al. (2009, 2012). Using height h_{TTD} and length l_{TTD} of the TTD, the numerical simulation will converge for $l_{TTD}/h_{TTD} \to \infty$ and $h_{TTD}/(t_{ox} + t_{met}) \to \infty$ towards the effective medium calculation. However, the measured resistance of the TTD is about 20% lower than theoretically expected. This might be caused by the inhomogeneous thicknesses of the hand-made Ag layers in the device stack. The measured output power increases steadily to 1 mW at $\Delta T = 37.4$ K. The simulation overestimates the power by a factor 1.2, the analytical expressions deviate by a factor of about 1.7. Figure 7 displays the figure of merit with calculated, simulated and measured data. The thermal conductivity λ_{yy} was calculated from the measured material properties. It is evident that as well here the FEM simulation closely reflects the measured data. The ratio of about 1.2 between the simulated and measured data is almost constant in

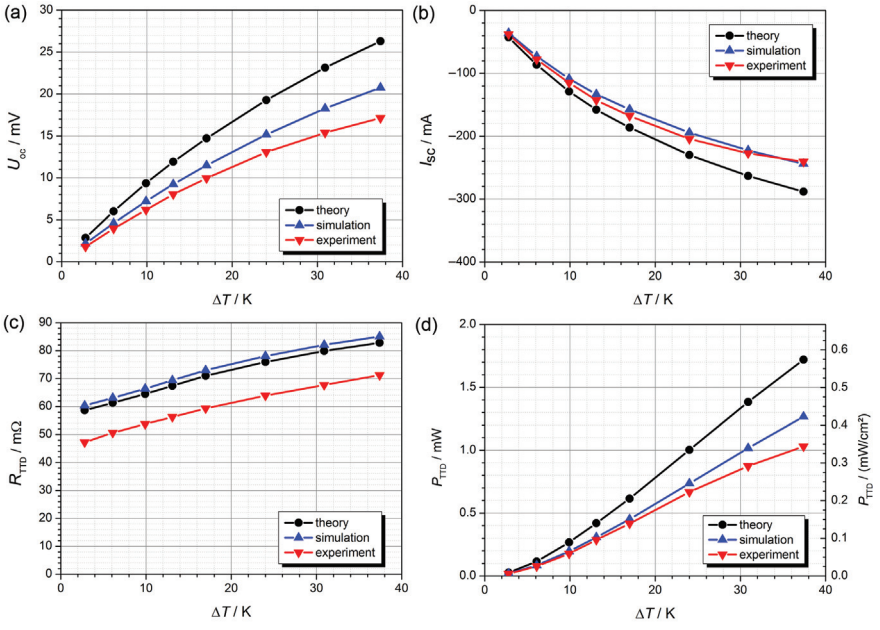

Figure 6: Electrical characteristics vs temperature difference of the TTD: (a) open circuit voltage U_{oc}, (b) short-circuit current I_{sc}, (c) electrical resistance R_{TTD} and (d) electrical power P_{TTD}.

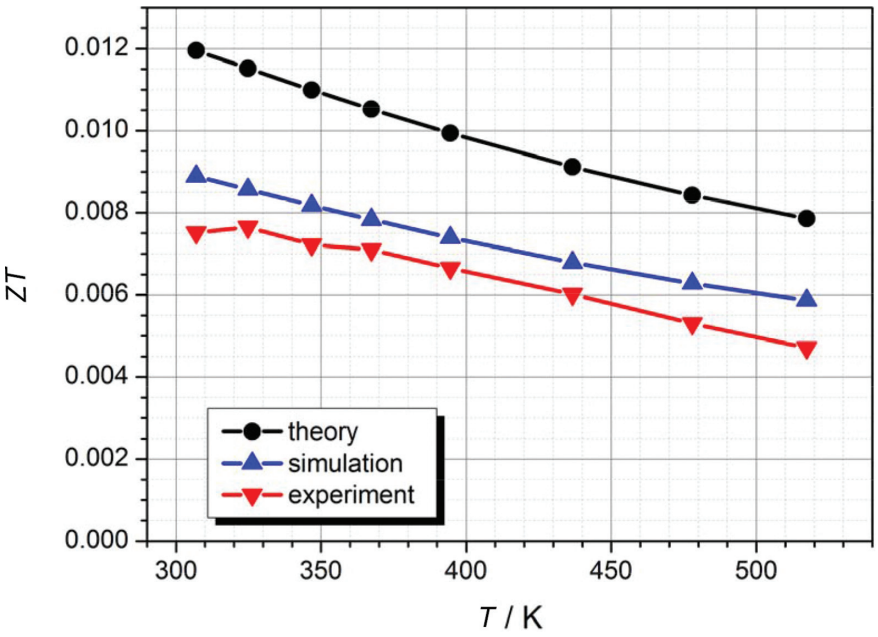

Figure 7: Dimensionless figure of merit of the transversal thermoelectric device vs temperature.

the investigated temperature range again proving the validity of the simulated data. However, here too the analytical expressions overestimate the real data in a significant way.

It should be noted that the test device is not optimized for a number of parameters such as the tilt angle or the thickness of the individual layers. Furthermore, the temperature differences realized so far could be increased significantly by active cooling of the device on the low temperature side. In order to estimate the output power at a higher temperature difference the FEM simulation was performed for the low temperature of 350 K and the temperature difference 300 K. The optimization of the tilt angle φ at the layer thickness ratio used yields an improvement factor of about 1.4 for the output power. Under these conditions the simulated power density becomes 40 mW/cm^2. As shown in Figure 6(d) the simulation overestimates the real output power by a factor 1.2 at the temperature difference of 37.4 K. However, even with a further significant increase in the deviation between simulation and experiment it can be expected that oxide-metal TTD will reach a power density which is comparable to data obtained for common dual leg devices, cf. the data summary given in Lim et al. (2012).

Summary and Conclusion

We have discussed device concepts of energy harvesters as dual leg, unileg and transversal thermoelectric devices based on an analytical approach for the figure of merit and on data published on oxide thermocouples. It has been shown that the mismatch of the oxide material properties reduces the figure of merit of the dual leg devices in many cases. Here, the unileg design including only one oxide and a metal may improve the expected performance. Furthermore, the unileg design was compared with a transversal setup resulting in an almost identical figure of merit for both types of devices. As a consequence it could be stated that the transversal thermoelectric device is always a simplified alternative if no pair of oxides with matching properties is available. Considering the potential application of a large-scale multilayer ceramic technology, it can further be concluded that the transversal device provides certain advantages compared to unileg devices. An oxide-metal transversal laboratory test device was built and characterized in detail to evaluate the potential of the oxide based transversal thermoelectric energy harvester. The results obtained allow the conclusion that transversal devices may deliver an electrical power density similar to recently published oxide dual leg devices. The generated power in particular will be sufficient to drive sensor or radio applications in the low power range. At the same time transversal devices should have significant advantages considering the conditions required for a large-scale production.

Funding: The work was financially supported within the project “THERMUMOX” by the Thuringian Ministry for Economy, Labour and Technology – European Social Fund Thuringia (2011FGR0132) and the project “NOXTHERMO” by the Federal Ministry of Education and Research Germany (03FH003I2).

References

Babin, V. P., T. S. Gudkin, Z. M. Dashevski, L. D. Dudkin, E. K. Iordanishvilli, V. I. Kaidanov, N. V. Kolomoets, O. M. Narva, and L. S. Stilbans. 1974. "Anisotropic Synthetic Thermoelements and Their Maximum Capabilities." *Soviet Physics: Semiconductors* 8: 478.

Cobble, M. H. 1995. "Calculation of Generator Performance." In *The Book CRC Handbook of Thermoelectrics*, edited by D. M. Rowe. Boca Raton London New York Washington, D.C.: CRC Press LLC.

Cusack, N., and P. Kendall. 1958. "The Absolute Scale of Thermoelectric Power at High Temperature." *Proceedings of the Physical Society* 72: 898.

Feldhoff, A., and B. Geppert. 2014. "A High-Temperature Thermoelectric Generator Based on Oxides." *Energy Harvesting and Systems* 1: 69.

Funahashi, R., A. Kosuga, N. Miyasou, E. Takeuchi, S. Urat, K. Lee, H. Ohta, and K. Koumoto. 2007. "Thermoelectric properties of $CaMnO_3$ system." In The book International Conference on Thermoelectrics, 2007. ICT 2007. 26th, IEEE.

Funahashi, S., T. Nakamura, K. Kageyama, and H. Ieki. 2011. "Monolithic Oxide-Metal Composite Thermoelectric Generators for Energy Harvesting." *Journal of Applied Physics* 109: 124509.

Funahashi, R., S. Urata, K. Mizuno, T. Kouuchi, and M. Mikami. 2004. "$Ca_{2.7}bi_{0.3}Co_4O_9/La_{0.9}bi_{0.1}NiO_3$ Thermoelectric Devices with High Output Power Density." *Applied Physics Letters* 85: 1036.

Gallo, C. G., B. S. Chandrasekhar, and P. H. Sutter. 1963. "Transport Properties of Bismuth Single Crystals." *Journal of Applied Physics* 34: 144.

Goldsmid, H. J. 1995. "Conversion Efficiency and Figure-of-Merit." In *The Book CRC Handbook of Thermoelectrics*, edited by D. M. Rowe. Boca Raton London New York Washington, D.C.: CRC Press LLC.

Goldsmid, H. J. 2012. "Transverse Thermoelectric Effects and Their Application." In *The Book Materials, Preparation and Characterization in Thermoelectrics*, edited by D. M. Rowe. Boca Raton: CRC Press, Taylor & Francis Group.

Gudkin, T. S., and E. É. Fiskind. 1978. "Response Time of a Thermal Converter with a Synthetic Anisotropy." *Soviet Technical Physics Letters* 4: 340.

Gudkin, T. S., E. K. Iordanishvili, and E. É. Fiskind. 1978. "Transverse Cooling Effect in a Stratified Medium with Artificial Anisotropy." *Soviet Technical Physics Letters* 4: 244.

Han, L., Y. Jiang, S. Li, H. Su, X. Lan, K. Qin, T. Han, H. Zhong, L. Chen, and D. Yu. 2011. "High Temperature Thermoelectric Properties and Energy Transfer Devices of $Ca_3co_{4-x}Ag_xO_9$ and $Ca_{1-y}Sm_yMnO_3$" *Journal of Alloys and Compounds* 509, 8970.

Hashimoto, H., T. Kusunose, and T. Sekino. 2009. "Influence of Ionic Sizes of Rare Earths on Thermoelectric Properties of Perovskite-Type Rare Earth Cobalt Oxides RCoO3 (R = Pr, Nd, Tb, Dy)." *Journal of Alloys and Compounds* 484: 246.

Hayashi, S. F., T. Nakamura, K. Kageyama, and H. Takagi. 2010. "Monolithic Thermoelectric Devices Prepared with Multilayer Cofired Ceramics Technology." *Japanese Journal of Applied Physics* 49: 096505.

Heraeus data sheet: Ag conductor paste for LTCC/DPIS. 2014. http://heraeus-circuits components.com/media/webmedia_local/media/datasheets/ltccmaterials/TC_7302_151211.pdf.

Ho, C. Y., R. W. Powell, and P. E. Liley. 1972. "Thermal Conductivity of the Elements." *Journal of Physical and Chemical Reference Data* 1: 279.

Imanaka, Y. 2005. *Multilayered Low Temperature Cofired Ceramics (LTCC) Technology*. 1st Edition. New York: Springer US.

Inagoya, A., D. Sawaki, Y. Horiuchi, S. Urata, R. Funahashi, and I. Terasaki. 2011. "Thermoelectric Module Made of Perovskite Cobalt Oxide with Large Thermopower." *Journal of Applied Physics* 110: 123712.

Ioffe, A. F. 1957. *Semiconductor Thermoelements and Thermoelectric Cooling*. London: Infosearch.

Kanno, T., A. Sakai, K. Takahashi, A. Omote, H. Adachi, and Y. Yamada. 2012. "Tailoring Effective Thermoelectric Tensors and High-Density Power Generation in a Tubular $Bi_{0.5}sb_{1.5}te_3$/Ni Composite with Cylindrical Anisotropy." *Applied Physics Letters* 101: 011906.

Kanno, T., K. Takahashi, A. Sakai, H. Tamaki, H. Kusada, and Y. Yamada. 2014. "Detection of Thermal Radiation, Sensing of Heat Flux, and Recovery of Waste Heat by the Transverse Thermoelectric Field." *Journal of Electronic Materials* 43: 2072.

Kanno, T., S. Yotsuhashi, A. Sakai, and H. Adachi. 2009. "Enhancement of Transverse Thermoelectric Power Factor in Tilted Bi/Cu Multilayer." *Applied Physics Letters* 94: 061917.

Lemonnier, S., C. Goupil, J. Noudem, and E. Guilmeau. 2008. "Four-Leg $Ca_{0.95}sm_{0.05}MnO_3$ Unileg Thermoelectric Device." *Journal of Applied Physics* 104: 14505.

Li, F., and J. -F. Li. 2011. "Effect of Ni Substitution on Electrical and Thermoelectric Properties of $LaCoO_3$ Ceramics." *Ceramics International* 37: 105.

Lim, C. H., S. M. Choi, W. S. Seo, and H. H. Park. 2012. "A Power-Generation Test for Oxide-Based Thermoelectric Modules Using p-Type $Ca_3Co_4O_9$ and n-Type $Ca_{0.9}nd_{0.1}MnO_3$ Legs." *Journal of Electronics Materials* 41: 1247.

Liu, H. Q., X. B. Zhao, T. J. Zhu, Y. Song, and F. P. Wang. 2009. "Thermoelectric Properties of Gd, Y Co-Doped $Ca_3Co_4O_{9+\delta}$." *Current Applied Physics* 9: 409.

Matsubara, I., R. Funahashi, T. Takeuchi, S. Sodeoka, T. Shimizu, and K. Ueno. 2001. "Fabrication of an All-Oxide Thermoelectric Power Generator." *Applied Physics Letters* 78: 3627.

Matula, R. A.. 1979. "Electrical Resistivity of Copper, Gold, Palladium and Silver." *Journal of Physical and Chemical Reference Data* 6: 1147.

Nakamura, Y., and S. Uchida. 1993. "Anisotropic Transport Properties of Single-Crystal $La_{2-x}Sr_xCuO_4$: Evidence for the Dimensional Crossover"." *Physical Reviews* B47: 8369.

Noudem, J. G., S. Lemonnier, M. Prevel, E. S. Reddy, E. Guilmeau, and C. Goupil. 2008. "Thermoelectric Ceramics for Generators." *Journal of the European Ceramic Society* 28: 41.

Ohtaki, M., K. Araki, and K. Yamamoto. 2009. "High Thermoelectric Performance of Dually Doped ZnO Ceramics." *Journal of Electronics Materials* 38: 1234.

Ohtaki, M., H. Koga, T. Tokunaga, K. Eguchi, and H. Arai. 1995. "Electrical Transport Properties and High Temperature Thermoelectric Performance of $(Ca_{0.9}M_{0.1})$ MnO_3 (M = Y,La,Ce, Sm,in,Sn,Sb,Pb,Bi)." *Journal of Solid State Chemistry* 120: 105.

Park, K., J. W. Choi, and C. W. Lee. 2009. "Characteristics of Thermoelectric Power Modules Based on p-Type Na $(Co_{0.95}ni_{0.05})_2O_4$ and n-Type $Zn_{0.99}sn_{0.01}o$." *Journal of Alloys and Compounds* 486: 785.

Park, K., and G. W. Lee. 2013. "Fabrication and Thermoelectric Power of π-Shaped $Ca_3Co_4O_9/CaMnO_3$ Modules for Renewable Energy Conversion." *Energy* 60: 87.

Reddemann, H. 1937. "Transversale Thermokraft in Einkristallen." *Annalen der Physik-Berlin* 29: 286.

Reitmaier, C., F. Walther, and H. Lengfellner. 2010. "Transverse Thermoelectric Devices." *Applied Physics A* 99: 717.

Schnellbögl, A., J. Betz, K. F. Renk, W. Prettl, H. Lengfellner, and G. Kremb. 1992. "Giant Voltages Upon Surface Heating in Normal Y $Ba_2Cu_3O_{7-\Delta}$ Suggesting an Atomic Layer Thermopile." *Applied Physics Letters* 60: 501.

Shin, W., and N. Murayama. 1999. "Li-Doped Nickel Oxide as a Thermoelectric Material." *Japanese Journal of Applied Physics* 38: L1336.

Shin, W., N. Murayama, K. Ikeda, and S. Sago. 2000. "Fabrication of Oxide Thermoelectric Generator Element." *Japanese Journal of Applied Physics* 39: 1254.

Snarskii, A. A., and L. P. Bulat. 2006. "Anisotropic Thermoelements." In *The Book CRC Thermoelectrics Handbook, Macro to Nano*, edited by D. M. Rowe. Boca Raton: CRC Press LLC.

Snarskii, A. A., A. M. Pal'ti, and A. A. Ascheulov. 1997. "Anisotropic Thermocouples Article." *Semiconductors* 31: 1101.

Su, H., Y. Jiang, X. Lan, X. Liu, H. Zhong, and D. Yu. 2011. "$Ca_{3-x}Bi_xCo_4O_9$ and $Ca_{1-y}Sm_yMnO_3$ Thermoelectric Materials and Their Power-Generation Devices." *Physica Status Solidi* A208: 147.

Takahashi, K., T. Kanno, A. Sakai, H. Tamaki, H. Kusada, and Y. Yamada. 2013. "Bifunctional Thermoelectric Tube Made of Tilted Multilayer Material as an Alternative to Standard Heat Exchangers." *Nature Scientific Reports* 3: 1501.

Terasaki, I., Y. Sasago, and K. Uchinokura. 1997. "Large Thermoelectric Power in $NaCo_2O_4$ Single Crystals." *Physical Review B* 56: R12685.

Tomeš, P., M. Trottmann, C. Suter, M. H. Aguirre, A. Steinfeld, P. Haueter, and A. Weidenkaff. 2010. "Thermoelectric Oxide Modules (TOMs) for the Direct Conversion of Simulated Solar Radiation into Electrical Energy." *Materials* 3: 2801.

Voigt, W. 1910. *Lehrbuch der Kristallphysik*. Leipzig: B. G. Teubner.

Wang, Y., Y. Sui, X. Wang, X., W. Su, and X. Liu. 2010. "Enhanced High Temperature Thermoelectric Characteristics of Transition Metals Doped $Ca_3Co_4O_{9+\Delta}$ by Cold High-Pressure Fabrication." *Journal of Applied Physics* 107: 033708.

Wang, L., M. Wang, and D. Zhao. 2009. "Thermoelectric Properties of c-Axis Oriented Ni-Substituted $NaCoO_2$ Thermoelectric Oxide by Citric Acid Complex Method." *Journal of Alloys and Compounds* 471: 519.

Yasukawa, M., and N. Murayama. 1998. "A Promising Oxide Material for High-Temperature Thermoelectric Energy Conversion: $Ba_{1-x}Sr_xPbO_3$ Solid Solution System." *Materials Science and Engineering* B54: 64.

Zhang, Y., and J. Zhang. 2008. "Rapid Reactive Synthesis and Sintering of Textured $Ca_3Co_4O_9$ Ceramics by Spark Plasma Sintering." *Journal of Materials Processing Technology* 208: 70.

Zhou, C., S. Birner, Y. Tang, K. Heinselman, and M. Grayson. 2013. "Driving Perpendicular Heat Flow: ($P \times$ n)-Type Transverse Thermoelectrics for Microscale and Cryogenic Peltier Cooling." *Physical Review Letters* 110: 227701.